Characterizing the information transmission of inverse stochastic resonance and noise-induced activity amplification in neuronal systems

Nataniel Martínez ●,[1,*] Roberto R. Deza,[1] and Fernando Montani ●[2]

[1]*IFIMAR (CONICET), Facultad de Ciencias Exactas y Naturales, Universidad Nacional de Mar del Plata, B7602AYL Mar del Plata, Argentina*

[2]*IFLP (CONICET), Facultad de Ciencias Exactas, Universidad Nacional de La Plata, B1900 La Plata, Argentina*

Purkinje cells exhibit a reduction of the mean firing rate at intermediate-noise intensities, which is somewhat reminiscent of the response enhancement known as "stochastic resonance" (SR). Although the comparison with the stochastic resonance ends here, the current phenomenon has been given the name "inverse stochastic resonance" (ISR). Recent research has demonstrated that the ISR effect, like its close relative "nonstandard SR" [or, more correctly, *noise-induced activity amplification* (NIAA)], has been shown to stem from the weak-noise quenching of the initial distribution, in bistable regimes where the metastable state has a larger attraction basin than the global minimum. To understand the underlying mechanism of the ISR and NIAA phenomena, we study the probability distribution function of a one-dimensional system subjected to a bistable potential that has the property of symmetry, i.e., if we change the sign of one of its parameters, we can obtain both phenomena with the same properties in the depth of the wells and the width of their basins of attraction subjected to Gaussian white noise with variable intensity. Previous work has shown that one can theoretically determine the probability distribution function using the convex sum between the behavior at small and high noise intensities. To determine the probability distribution function more precisely, we resort to the "weighted ensemble Brownian dynamics simulation" model, which provides an accurate estimate of the probability distribution function for both low and high noise intensities and, most importantly, for the transition of both behaviors. In this way, on the one hand, we show that both phenomena emerge from a metastable system where, in the case of ISR, the global minimum of the system is in a state of lower activity, while in the case of NIAA, the global minimum is in a state of increased activity, the importance of which does not depend on the width of the basins of attraction. On the other hand, we see that quantifiers such as Fisher information, statistical complexity, and especially Shannon entropy fail to distinguish them, but they show the existence of the mentioned phenomena. Thus, noise management may well be a mechanism by which Purkinje cells find an efficient way to transmit information in the cerebral cortex.

I. INTRODUCTION

During sleep, anesthesia, and quiet wakefulness, brain activity oscillates between decreasing and increasing states [1,2]. This behavior is observed as low-frequency activity (0.5–1.0 Hz) with large-amplitude delta waves [1]. The frequency of communication between the two states varies widely in conscious and anesthetized animals *in vivo*, and in both cases is known as bistability in a fraction of Purkinje cells [1].

Purkinje cells are a type of gamma-aminobutyric acid (GABA)-ergic neurons that produce most of the output of the cerebral cortex, the outer layer of the cerebellum, and are found in the cerebral cortex of all vertebrates. Each cell has a single axon that sends impulses to the region of the brain that controls movement and plays an important role in motor control and learning [1,2]. They are the only cells that transmit signals from the cerebellar cortex while receiving impulses from hundreds of thousands of cells, in addition

to having a high rate of action potential production and intrinsic bistability [1]. Therefore, it is important to understand how Purkinje cells handle information during bistability behavior [3].

In recent years, various research has suggested that noise may have a significant impact on neuronal dynamics [4–9]; for instance, moderate noise can raise inputs closer to a threshold and thereby induce the neuron to fire an action potential. On the other hand, a very high noise level does not help to create an action potential since it passes the potential barrier [5–9].

More recently, unusual behavior characterized by a minimization of the average spiking activity for an optimal amount of noise has been reported, which has prompted several theoretical studies [3,10–14]. This phenomenon was recently discovered in neuronal populations using biophysically realistic [15] models and various network coupling strategies [16].

Previously, part of the physics and engineering scientific community studied various implications of noise, where it fulfilled the role of building and enriching the stochastic dynamics of nonlinear systems [17–19]. The occurrence of this phenomenon is subject to the specifics of the nonlinear potential to which the system is subjected. To illustrate,

consider a particle that can move through a bistable potential subjected to an external stochastic force. Depending on its initial state, the particle is in one of the minima where, if the intensity of the force causes the behavior of alternation from one of the minima to the other, it is called stochastic resonance (SR) [20–24]. If these minima now have different activities and the transition from a low-activity to a high-activity minimum takes place, a so-called noise-induced activity amplification (NIAA), also known as a nonstandard stochastic resonance, is generated [25]. However, if the opposite occurs, i.e., a transition from a state of greater to a state of lesser activity, this is referred to as inverse stochastic resonance (ISR) [26].

Although the aforementioned nomenclature was adopted by the neuroscientific community, it is just an analogy that aids in comprehending the significance of noise in brain systems. One of the first experimental evidence of ISR is an *in vitro* preparation of Purkinje brain cells [3], which demonstrates that ISR allows cells to operate in "alternative functional regimes" (all-or-none toggle or the linear filter mode). Furthermore, ISR is thought to be crucial in computational mechanisms that need less firing activity without pharmacological inhibitory neuromodulation (or, alternatively, when other computational mechanisms require bursts of on-off activity). The NIAA phenomenon, on the other hand, is far more challenging to separate from ISR, yet it turns out to be merely one facet of the mechanism that causes ISR. Both phenomena are currently very active research topics [27–30].

Recently, a model that explains the development of the ISR behavior has been published, and it contains certain significant components that earlier studies have identified as the cause of noise-induced activity amplification [26]. In particular, as there is a distribution of the initial conditions, the coexistence of a stable resting equilibrium and a stable spiking limit cycle (i.e., oscillatory state coexists) in neuron dynamics. This demonstrates how the essence of ISR differs from SR, where the initial conditions are irrelevant [7,11]. The procedures employed to identify the occurrence of ISR and NIAA, however, are important.

The behavior of a bistable oscillatory system can be reduced to a model of firing rate equations, i.e., the number of spikes fired per unit time [31], whose dynamics is controlled by a function of nonequilibrium potential (NEP) (see, e.g., Refs. [32–34]), so that the bistability between a limit cycle and a quiescent state is reduced to a bistability between two fixed points in such rate models, one of which corresponds to a high firing rate and the other to a very small or zero firing rate. The model proposed in [26] assumes a single variable x representing the *activity* of the system, subject to a potential with two local minima—a "down" or low-activity state and an "up" or high-activity state—where the down state is globally stable but has a sensibly narrower basin of attraction than the metastable up state.

Knowledge of the nature of ISR and NIAA behavior can provide locally optimal information about the input and output sets of Purkinje cells. Therefore, in this article, we discuss whether the relationship between the lengths of the basins of attraction between the rising and falling states affects the formation of the ISR and NIAA behavior, using the symmetry

TABLE I. Parameter sets leading to regimes displaying the phenomenon.

	ISR	NIAA
a	2	2
b	2.999	−2.999
c	1.4	1.4
d	−3.496	3.496
x_0	0.435	−0.435

feature underlying the asymmetric potential function in [26]. Furthermore, on the one hand, although NIAA behavior is little studied in the literature, in this paper we deepen its analysis and show that it is a behavior with certain characteristics similar to ISR. We also show that the mean firing rate exhibits the same characteristic behavior of both phenomena.

On the other hand, we extend the analysis of these phenomena by studying the behavior of the quantities provided by information theory, which allows us to have multiple quantifiers, i.e., measures that can characterize a particular property of the probability distribution function associated with a time series related to a physical observation such as the activity x of Purkinje cells. Specifically, we use three quantifiers: The Shannon entropy, which gives us an idea of how disordered the system is; the Fisher information, which gives us an idea of how much information the system provides; and the statistical complexity, which tells us how complex the system is. In order to apply these quantifiers, one needs to know the probability distribution function for which analytical approximations are available in the small- and high-noise limits, respectively [26]. We use the "weighted-ensemble Brownian dynamics simulation" (WEBDS) method that allows us not only to obtain the expression of the probability in the mentioned limits, but also for intermediate-noise intensities.

II. METHOD

A. The potential function

Purkinje cells have the peculiarity that their axons are the only projection from the cerebellar cortex to deeper cerebellar structures. They have complex internal dynamics which allow them to fire spontaneously and display bistability. Bistability has also been observed in various cellular behaviors [35], and to understand it we consider a one-dimensional system such that their state or activity can be described by means of a variable $x(t)$ whose dynamics is given by

$$\frac{dx}{dt} = -\frac{\partial \varphi(x)}{\partial x}, \tag{1}$$

where the potential $\varphi(x)$ belongs to a class of familiar models in chemical kinetics [36–38], which was also used in [26], and has the form

$$\varphi(x) := a \arctan[b(x + x_0)] + c(x + x_0)^2 + d(x + x_0). \tag{2}$$

Different combinations of the parameters of the potential $\varphi(x)$ show different bistable behavior, of which we highlight the combinations of the parameters from Table I shown in Fig. 1. Both scenarios exhibit a bistable behavior with two
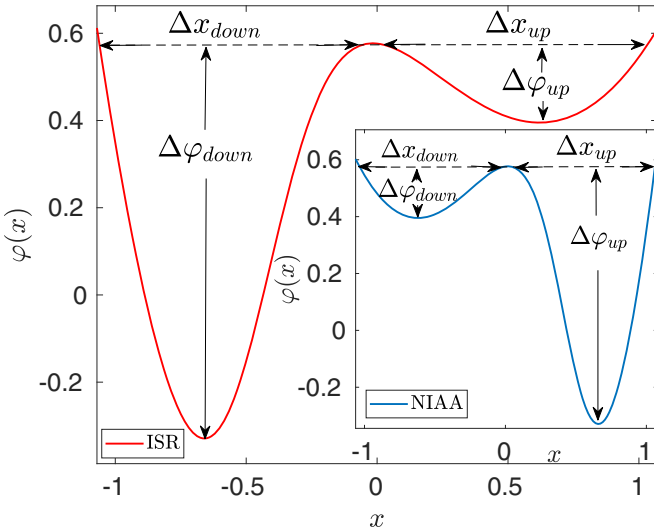
FIG. 1. Potential $\varphi(x)$ for the ISR (red line) and NIAA (blue line) cases for the parameter values according to Table I. In both curves, they have a potential with two local minima: A "down" or low-activity state and an "up" or high-activity state. Each minimum has an attraction basin, Δx_{down} and Δx_{up}, and potential barrier, $\Delta\varphi_{\text{down}}$ and $\Delta\varphi_{\text{up}}$, corresponding to the state down and up, respectively. Note that the stable and metastable minima have the same values in the potential for ISR and the one for NIAA.

minima that can be observed in both cases, i.e., a global (larger $\Delta\varphi$) and a metastable (lower $\Delta\varphi$) minimum. In particular, for the red potential, these minima are in a state of low ($\Delta\varphi_{\text{down}}$) and high ($\Delta\varphi_{\text{up}}$) activity, respectively, while for the blue potential, the global minimum is in a state of high activity ($\Delta\varphi_{\text{up}}$) and the metastable minimum is in a state of low activity ($\Delta\varphi_{\text{down}}$).

The symmetry is what we highlight in terms of the potential when we contrast the parameters b, d, and x_0, which allows us to obtain the same magnitudes for each minimum in both $\Delta\varphi$ and Δx, that is, red $\Delta\varphi_{\text{down}}$ = blue $\Delta\varphi_{\text{up}}$ and red $\Delta\varphi_{\text{up}}$ = blue $\Delta\varphi_{\text{down}}$, with the particularity $\Delta x_{\text{down}} = \Delta x_{\text{up}}$ for both potentials. Thanks to this property, we can find different behaviors of the potential for different variants of the phenomenon by varying only the parameter c, which gives us three variants for the size of the basins: $\Delta x_{\text{down}} > \Delta x_{\text{up}}$, $\Delta x_{\text{down}} = \Delta x_{\text{up}}$, and $\Delta x_{\text{down}} < \Delta x_{\text{up}}$. As we can see in Fig. 2, for $c = 1.5$, the black lines allow us to see $\Delta x_{\text{down}} > \Delta x_{\text{up}}$ for the ISR case and $\Delta x_{\text{down}} < \Delta x_{\text{up}}$ for the NIAA case; for $c = 1.3$, the orange lines show $\Delta x_{\text{down}} < \Delta x_{\text{up}}$ for ISR and $\Delta x_{\text{down}} > \Delta x_{\text{up}}$ for NIAA; and for the case $c = 1.4$, the same graph is reproduced as in Fig. 1, where the basins are $\Delta x_{\text{down}} = \Delta x_{\text{up}}$.

To study the dynamics of the potential φ, we will consider the behavior of this system under the action of a noise source whose time evolution is described by the one-dimensional Langevin equation,

$$\frac{dx}{dt} = -\frac{\partial\varphi(x)}{\partial x} + \eta(t). \quad (3)$$

We assume here that the noise has the form of an additive Gaussian term $\eta(t)$ with zero mean $\langle\eta(t)\rangle = 0$ and autocorrelation $\langle\eta(t)\eta(t')\rangle = 2D\delta(t - t')$.
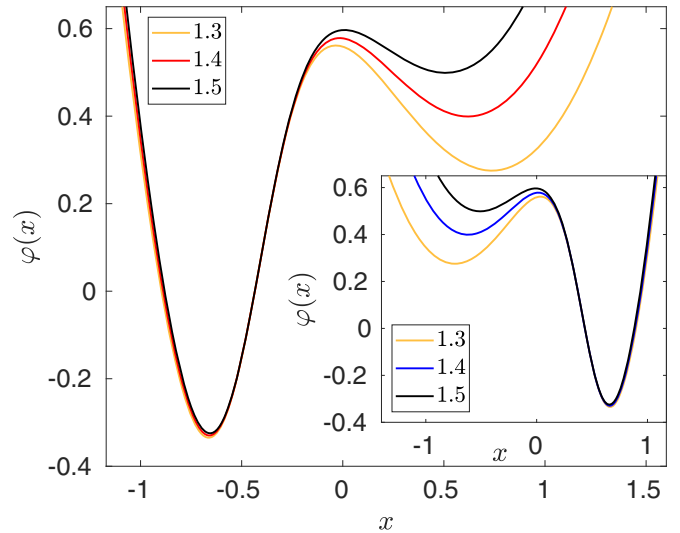
FIG. 2. ISR behavior (main graph) and NIAA (inset) for three values of the parameter c, which represent three relationships between the basins, which are $\Delta x_{\text{down}} > \Delta x_{\text{up}}$ for the black line, $\Delta x_{\text{down}} = \Delta x_{\text{up}}$ for the red line, and $\Delta x_{\text{down}} < \Delta x_{\text{up}}$ for the orange line, in the ISR case, as opposed to the NIAA case, which are $\Delta x_{\text{down}} > \Delta x_{\text{up}}$ for the orange line, $\Delta x_{\text{down}} = \Delta x_{\text{up}}$ for the blue line, and $\Delta x_{\text{down}} < \Delta x_{\text{up}}$ for the black line. The different ISR and NIAA potentials are symmetrical, i.e., they have the same magnitudes, but the minima are reversed.

To understand the behavior of ISR, we imagine a set of particles that evolve in the potential φ whose dynamics evolves according to the Langevin equation [Eq. (2)]. At first, for noise values D very close to zero, the particles start in the initial conditions; even if a long enough time t passes, the particles will always be around their initial positions (small disturbances caused by noise practically do not displace the particles), so $\langle x \rangle$ are just the average values of the initial positions. For moderate noise values, some of the initial conditions falling into the metastable state basin of attraction may be sufficiently perturbed to overcome the $\Delta\varphi_{\text{up}}$ barrier and reach the stable minimum. But, on the other hand, the initial conditions falling within the basin of attraction of the stable minimum are perturbed, but not enough to overcome the $\Delta\varphi_{\text{down}}$ barrier, so it remains at that minimum. In this way, the noise perturbations push the particles out of the metastable state and evolve to the stable state, decreasing the value of $\langle x \rangle$. As the noise intensity increases, the probability increases that a particle will cross the potential barrier $\Delta\varphi_{\text{down}}$ in a finite time t and it evolves to a state of greater activity, increasing the mean value $\langle x \rangle$.

Although the noise intensity in the NIAA case behaves as in the ISR case at values close to zero and at high values, at moderate values of D the particles manage to overcome the smallest barrier, which in this case is the down state. Thus, some of the particles reach the up state, which has a higher potential barrier that they cannot overcome at this noise intensity. So they remain trapped in this state, which causes the increase of the mean activity $\langle x \rangle$.

To better interpret the behavior of the mean activity as a function of noise intensity, we analyze Fig. 3, in which, for low values of noise intensity ($\sim 10^{-2}$), the perturbations are so
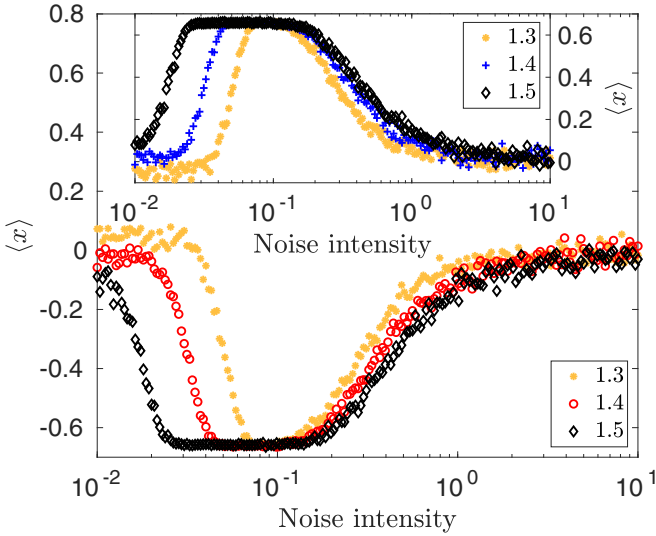
FIG. 3. Mean firing $\langle x \rangle$ as a function of noise intensity D for ISR (main image) and NIAA (inset). We can observe the characteristic behavior of both phenomena at intermediate intensity: In the case of ISR, a decrease in the activity $\langle x \rangle$, and in the case of NIAA, an increase in the average activity $\langle x \rangle$. The simulations were performed for $\Delta t = 2 \times 10^3$ in an arbitrary time unit and 1000 different initial conditions uniformly distributed over the interval $[-1.3, 1.3]$.

small that the particles cannot overcome any potential barrier, which shows a behavior of x close to zero since the particles are thrown uniformly and, on average, the same number of particles falls into each basin. As the intensity increases, more and more particles manage to overcome the barriers of the metastable state, with lower activity in the ISR case and higher activity in the NIAA case. At values of noise intensity $\sim 10^{-1}$, the perturbation is strong enough so that most particles succeed in reaching the stable minimum, but it is not intense enough to overcome the barrier, so the average of the activity is practically the value of the stable minimum. At intensity values $> 10^{-1}$, the particles can overcome this barrier so that they reach the metastable state and thus a return to the mean intensity value is observed. At very high intensity values, the particles can be anywhere in the potential.

The most important thing in Fig. 3 is the characteristic behavior of the decrease in mean activity for ISR and the increase in mean activity for NIAA, not only when the basin of the metastable minimum is larger than the basin of the stable minimum, but also for three relationships of the size of the basins of attraction, as can be seen for $c = 1.3$ where $\Delta x_{\text{down}} < \Delta x_{\text{up}}$ for ISR and $\Delta x_{\text{down}} > \Delta x_{\text{up}}$ for NIAA, or for $c = 1.4$, where $\Delta x_{\text{down}} = \Delta x_{\text{up}}$ for both ISR and NIAA, and for $c = 1.5$, where $\Delta x_{\text{down}} > \Delta x_{\text{up}}$ for ISR and $\Delta x_{\text{down}} < \Delta x_{\text{up}}$ for NIAA.

Looking at the different curves of the $\langle x \rangle$ in Fig. 3 for values of noise intensity, two differences can be observed for the different values of c. On the one hand, the initial difference in the mean value of the activity $\sim 10^{-2}$, which is due to the fact that for $c = 1.4$, the minima are practically symmetrically arranged and show a mean behavior of the activity very close to zero, while for $c = 1.3$, the basin of the metastable state widens and shifts the location of the minimum away from

zero, causing it to be more significant in the calculation of the mean value of the activity. The opposite happens in the case of $c = 1.5$, where the basin of the metastable minimum is smaller and the minimum moves closer to zero, which is less relevant in the calculation of the average value of the activity.

On the other hand, the difference in the onset of decay (ISR) or increase (NIAA) of the mean activity for stronger values of noise intensity is due to the fact that as the value of c decreases, the barrier of the metastable state increases, which means that the perturbations required to overcome this barrier must be larger.

To find a theoretical expression for the behavior of the mean of the activity, in [26] the authors propose a convex combination, i.e., a hyperbolic tangent function that depends on D and is bounded by a factor D_0 separating two behaviors: Between the behavior for high values of the noise intensity, expressed by the Fokker-Planck equation [39], which explains the behavior for values of $(D > 10^{-1})$, and between low amplitudes of the noise expressed by the Kramer escape rate [40], which correctly explains the behavior for $D < 10^{-1}$. In Sec. II C, we will see that the WEBDS method not only correctly indicates both behaviors, but also the transition between them, which makes it possible to determine the probability distribution function (PDF) value more reliably.

B. Firing rate

We consider the firing rate as the average number of oscillations during a long period of time, which corresponds to calculating the number of particles that pass from a down state to an up state, depending on the noise intensity. Or, analogously, we can consider a set of uncoupled neurons that can be in an off state (down state) or an on state (up state) from which they can oscillate, depending on the noise intensity.

To calculate the average firing rate, we first consider 10^4 particular instances of a network of 10^4 uncoupled neurons evolving 10^5 arbitrary units of time under the action of the potential $\varphi(x)$. In Figs. 4(a) and 4(b), we see the behavior of the average firing rate for ISR and NIAA, respectively, and for the three combinations of the basin of attraction, where not only are they the same characteristic behaviors found for each phenomenon, but they also occur for the three variants of the basins of attraction.

In the upper panel of Fig. 4, we see how the average firing rate reflects the characteristic behavior for both ISR in Fig. 4(a) and NIAA in Fig. 4(b). At very low values of noise intensity ($\sim 10^{-2}$), the neurons spend on average the same time in the low- and high-activity state, as they are initially normally distributed between these states. As noise intensity increases, neurons may be deactivated for ISR or activated for NIAA, which occurs at intensities around $\sim 2 \times 10^{-2}$ as a function of the value of c because, as the value of this parameter increases, the differences between $\Delta \varphi_{\text{down}}$ and $\Delta \varphi_{\text{up}}$ become more pronounced, so that a higher intensity is required to activate the same number of neurons. At an intensity ($5 \times 10^{-2} < D < 1 \times 10^{-1}$), the group of neurons succeeds in completely shutting down (ISR) or turning on (NIAA). However, at intensities above 10^{-1}, the neurons change state again and enter a fluctuation between the two possible states that even exceeds the original distribution for 10^0.
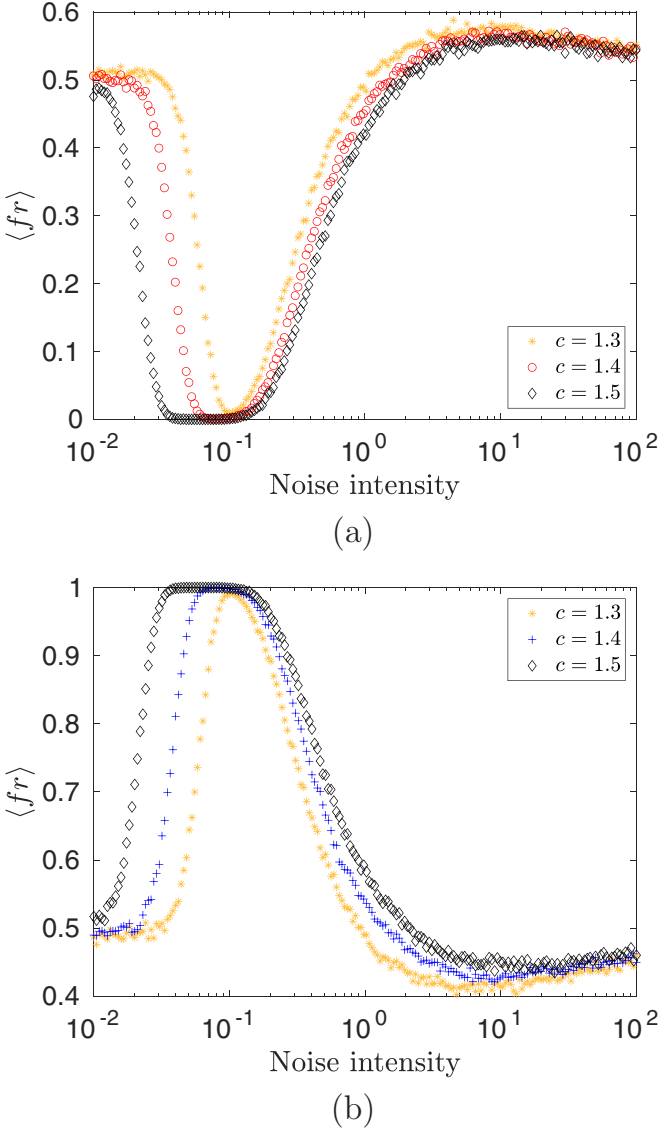
FIG. 4. Mean firing rate as a function of noise intensity for the behaviors (a) ISR and (b) NIAA for different values of parameter c. In both figures, it can be seen that the behavior of the average firing rate follows the characteristic behavior of both phenomena and is independent of the relationship between the basins.

C. Weighted-ensemble Brownian dynamics simulation

A very effective method for the calculation of the probability density function of Brownian particles moving in a potential landscape was proposed in [41], where the authors start from the weighted-ensemble Brownian dynamics simulation method but use a uniform distribution of walkers within each subregion, so that when moving to the underlying dynamics the walkers transport probability between the subregions, which allows the calculation of low probabilities and low rates.

We are interested in numerically finding the stationary probability density $p_{st}(X_j)$ of the particles position M_{res} evenly spaced supporting points X_j in a finite part of the physical space given by $x \in [L^-, L^+]$. The region of interest is divided into $M > M_{res}$ subregions of size $\Delta x = \frac{L^+ - L^-}{M}$, where
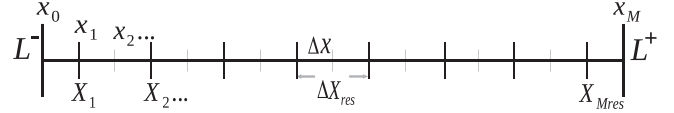
FIG. 5. Scheme that explains the divisions of space to calculate the PDF. The spacing is such that $x \in [L^-, L^+]$ is divided into a set M such that $\Delta x = \frac{L^+ - L^-}{M}$ with a subdivision M_{res} of points X_j such that $\Delta X_{res} = \frac{M}{M_{res}} \Delta x$.

the ith subregion is bounded by (x_i, x_{i+1}), $i = 0, \ldots, M-1$, with $x_i = i\Delta x + L^-$. Supporting points are given explicitly by $X_j = L^- + (j - 1/2)\Delta X_{res}$, $j = 1, 2, \ldots, M_{res}$, with $\Delta X_{res} = \frac{M}{M_{res}}$, as we can see in Fig. 5.

Following the initial setting of $\mathbf{P}(t = 0)$, the time evolution of the $\mathbf{P}(t) \to \mathbf{P}(t + h)$ is carried out in three steps using integration time step h:

Redistribution. N walkers (copies of the system) are uniformly distributed in each subregion. Besides their individual positions $x_i^k(t)$, where $i = 0, \ldots, M-1$ denotes the particular subregion and $k = 1, \ldots, N$ the individual walkers, each walker possesses a given amount of weight $q_i^k(t)$. This is simply the present probability in the ith subregion distributed to the N walkers, which yields $q_i^k(t) = p_i(t)/N$.

Integration. Using integration time step h, Heun's integration model is employed with white noise. This integration step realizes the time evolution $x_i^k(t) \to x_i^k(t + h)$. Here, walkers transport probability between the subregions. As walkers are independent of each other, it is important to note that the particular time evolution of each one of the N walkers is due to different sample paths in the stochastic parts of the Langevin equation.

Updating. Compute $P_i(t) \to P_i(t + h)$ by summing up the weights of all walkers that are currently located in the particular subregion.

In what follows, we name the sequence of redistribution, integration, and updating steps as the running step. After the number of integration time steps used for equilibration, T_{therm}, the set $\mathbf{P}(t)$ (with $\mathbf{P}(t) = [P_0(t), P_1(t), \ldots, P_{M-1}(t)]$) reaches a stationary regime where the $P_i(t)$'s fluctuate around their mean values $\langle P_i \rangle$. The individual $\langle P_i \rangle$ values are estimated by averaging over a total amount of N_T sets, $\mathbf{P}(t_l)$, $l = 1, 2, \ldots, N_T$, taken after the system has reached the stationary regime. Finally, the PDF on the supporting points $p_{st}(X_j)$ is calculated by adding the adjacent $\langle P_i \rangle$ and dividing by the size ΔX_{res} (in order to have a properly normalized PDF),

$$p_{st}(X_j) = \frac{1}{\Delta X_{res}} \sum_{i=(j-1)\frac{M}{M_{res}}}^{j\frac{M}{M_{res}}-1} \langle P_i \rangle. \tag{4}$$

Due to the redistribution step, where walkers are uniformly distributed in each subregion, statistical errors occur because they may reach positions in a subregion that are inaccessible or, at least, more improbable, leading to a flattening of the probability distribution, i.e., leading to more probability in regions of low probability. To solve this problem, the authors show that the determination of lower time steps allows one to sample regions far from the potential extrema, having to comply to fulfill specific criteria for the time step h and the

size of a subregion, Δx. To satisfy the WEBDS integration criteria, we use symmetric Δx intervals (i.e., $L^- = -L^+$); changing the parameter x_0 in this way, we define the intervals $[L^-, L^+]$ for $c = 1.3$ with $L^+ = 1.17$ and $x_0 = 0.535$, $c = 1.4$ with $L^+ = 1.07$ and $x_0 = 0.435$, and $c = 1.5$ with $L^+ = 0.97$ and $x_0 = 0.34$. Consider that for the NIAA potential, the negative value of x_0 is taken into account. From now on, the potentials with these values for the parameters x_0 and Δx will be considered.

To perform the simulation, we first consider $P_0(x_i) = \frac{1}{M}$ for $N = 2$ walkers considering a division of the integration space of $M = 3000$ with a subdivision of $M_{res} = 200$, with integration time step of $h = \frac{2D}{250}$, and considering a thermalization time of $T_{therm} = \frac{500}{h}$. After this simulation time has elapsed, it is averaged over the N samples of the distribution taken every $n_{av} = 10$ time steps. For large values of the noise intensity, the perturbations are high so the particles can be in any state of the system, which leads to the thermalization time being sufficient to achieve seasonality, corresponding to a behavior similar to that described by the Fokker-Planck equation. On the other hand, as the noise intensity decreases, the thermalization time increases, but for noise values ($D < 10^{-1}$), the perturbations are small, requiring a longer thermalization time to achieve seasonality.

To better understand this process, we show Fig. 6 depicting the behavior of $-D \ln P$, for both ISR [Fig. 6(a)] and NIAA [Fig. 6(b)] in two particular cases of D, for which it satisfies the transition between the behavior between high and low intensities, for the parameters described in Table I. In both Figs. 6(a) and 6(b), we compare the estimates of the behavior of the stationary probability density described by Fokker-Planck (solid line) with the data of the WEBDS method (black circles) and the representation of the probability calculation for the case of 1000 particles, which follows the Langevin behavior (squares). As can be seen in Fig. 6(a) ($D = 0.089$), the three curves describe the same behavior corresponding to strong noise, which are different from values of $D = 0.055$ where we enter the behavior for low noise, in which the Fokker-Planck behavior is not representative and the proposed WEBDS model describes Langevin behavior very well for both phenomena.

For the case of higher values of noise intensity ($D > 10^{-1}$), the three curves follow the same behavior since seasonality has already been achieved for the Langevin case and the perturbations caused by the noise are larger, so the thermalization time specified in WEBDS is sufficient to achieve seasonality (i.e., $|\Delta\varphi_{down} - \Delta\varphi_{up}|$ is maximum). However, for lower values of noise intensity ($D < 8 \times 10^{-2}$), the probability of finding particles in the metastable minimum increases (i.e., $|\Delta\varphi_{down} - \Delta\varphi_{up}|$ decreases), moving away from the Fokker-Planck behavior, as seen in Fig. 6(b). As the noise intensity continues to decrease ($D \sim 10^{-2}$), the probability of finding particles in the metastable minimum resembles the probability of the steady state (i.e., $|\Delta\varphi_{down} - \Delta\varphi_{up}|$ is minimal) described by the Langevin equation, which can be reproduced by the WEBDS method.

D. Information theory

The quantifiers provided by information theory correspond to measurements capable of characterizing a given property of
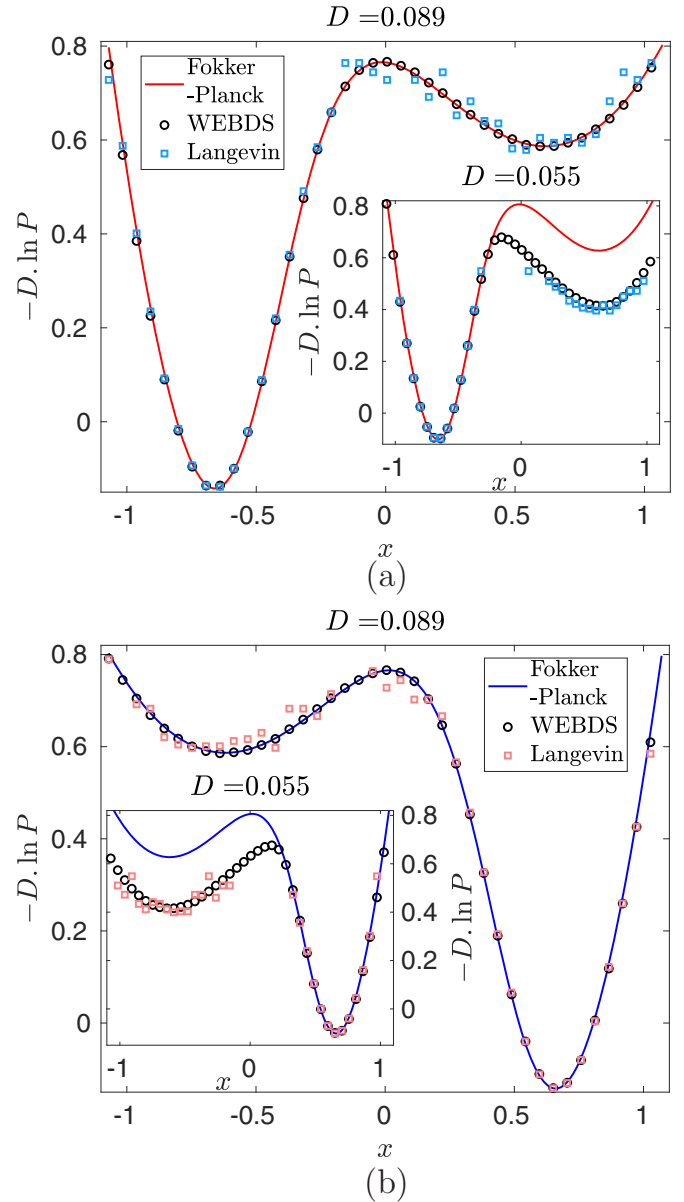
FIG. 6. Verification of the operation of WEBDS (black circles) for values of noise intensity in the high-noise-intensity region (main graph) and in the low-intensity region (inset) for the cases (a) ISR and (b) NIAA. The squares correspond to the calculation of the probability when considering 1000 particles subject to the Langevin dynamics, while the solid lines correspond to the Fokker-Planck behavior.

the probability function associated with a time series related to a physical observation, such as the behavior of a particle subject to a bistable potential.

1. Shannon entropy

One of the first quantifiers presented is the Shannon entropy [42], which is used to study stochastic resonance systems [43,44] or, currently, in various fields [45,46]. Entropy can be interpreted as a measure of the "degree of disorder" or uncertainty of whether a system is in a particular state.
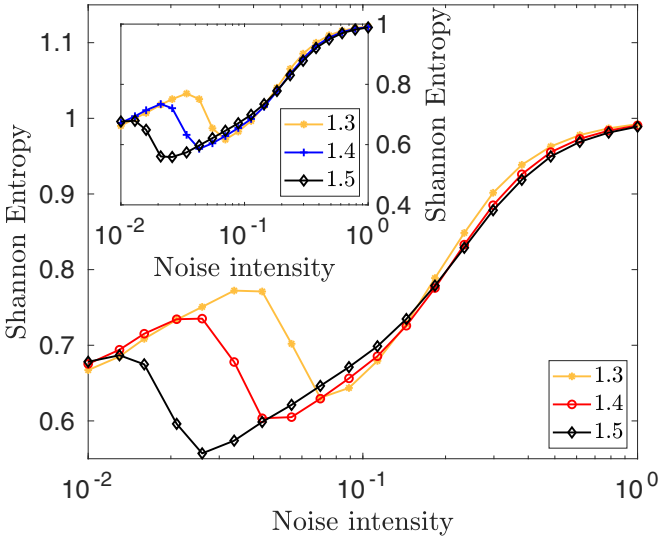
FIG. 7. Shannon entropy vs noise intensity for the ISR (main graph) and NIAA (inset) regimes, respectively. For both phenomena and different basin size ratios, a slight increase followed by a decrease in entropy is observed in the low-noise-intensity regime ($10^{-2} < D < 10^{-1}$).

Consider a discrete random variable X, the state space $\mathcal{X}$ of X, and the probability density function $p(x) = P(X = x)$ of X. The entropy $S[X]$ of a discrete random variable X is defined by

$$S[X] = -\sum_{x \in \mathcal{X}} p(x) \log [p(x)]. \tag{5}$$

Note that Shannon entropy is a function of the distribution of X and does not depend on the values that the variable X takes, but rather on the probabilities. For our case, we will consider the Shannon entropy in its normalized version $S[X] = S[X]/S_{\max}$ since it has a "global character" as a quantifier of information because it does not react to small perturbations in the values or to the rearrangement of the components $p(x)$.

The behavior of Shannon entropy can be seen in Fig. 7 for three values of the parameter c when the ISR (main graph) and NIAA (inset) requirements are satisfied with respect to the intensity of the noise. In both cases, it can be observed that the entropy grows as long as the barrier of the metastable state is not overcome ($D \sim 1.3 \times 10^{-2}, D \sim 2.1 \times 10^{-2}$, and $D \sim 3.4 \times 10^{-2}$ for $c = 1.3, 1.4$, and 1.5, respectively), until reaching the value of the noise intensity at which the particles manage to escape from the metastable minimum and reach the stable minimum, showing an ordering of the particles or a decrease in entropy. As the noise intensity increases but is not high enough to break out of the stable minimum, entropy increases almost linearly to the point $D \sim 1.8 \times 10^{-1}$. At larger values, the entropy changes behavior and grows exponentially until it reaches its maximum value.

Despite the fact that Shannon entropy is a measure of the average uncertainty in the random variable, the behavior is the same for different ratios of the size of the attraction basins as well as for both phenomena. From now on, the representation criteria of the ISR and NIAA behaviors are maintained in the main graph and inset, respectively, against three values of the

parameter c that allow the comparison between the basins of attraction.
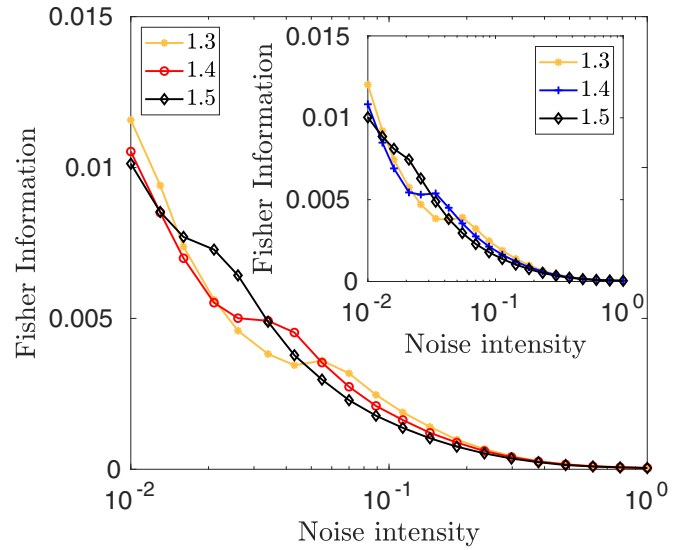
FIG. 8. Fisher information vs noise intensity for the ISR and NIAA regimes, respectively. Fisher's behavior quickly tends to zero, in contrast to the behavior of Shannon's entropy behavior.

2. Fisher information

Contrary to Shannon entropy, the Fisher information measure is particularly sensitive to substantial changes in PDF within a short region, allowing one to characterize the degree of disorder in a system or phenomena [47]. It is defined as [48]

$$F[\psi] = 4 \int |\overrightarrow{\nabla} \psi|^2 \, dx. \tag{6}$$

The presence of the gradient is responsible for the sensitivity of this quantizer to small perturbations of the probability density function, which is why it is called "local."

Considering the probability function $P = \{p_i, \ i = 1, \ldots, N\}$, corresponding to a discrete random variable X, where N is the number of possible states of the system, we can consider the Fisher normalized discrete information [49] given by

$$F[P] = F_0 \sum_{i=1}^{N-1} [\sqrt{p_{i+1}} - \sqrt{p_i}]^2, \tag{7}$$

where F_0 is a normalization constant,

$$F_0 = \begin{cases} 1 & \text{if } p_{i^*} = 1 \text{ for } i^* = 1 \text{ or} \\ & i^* = N \text{ and } p_i \neq 0 \ \forall i \neq i^*, \\ \dfrac{1}{2} & \text{opposite case.} \end{cases} \tag{8}$$

Plotting the behavior of Fisher information, as seen in Fig. 8, a rapid decay to zero is observed, with a slight increase in the interval where the characteristic decay or increase in ISR and NIAA phenomena occurs.

3. Statistical complexity

Finally, we consider the statistical complexity, which is able to quantify critical details of the dynamic processes underlying the system under study. For this reason, it is considered as a quantifier of information theory, indicating the "order" that systems possess [50].

Different definitions of statistical complexity are used, mainly because they use different definitions of standard entropies[50–57]. The main problem is that this ignores the fact that we are dealing with a probability space, and therefore it ignores the stochastic nature of the distributions [55]. To account for the stochastic nature of the data, in this article we choose a measure of disequilibrium based on the Jensen-Shannon divergence $\mathcal{D}_{JS}$ [56–59],

$$\mathcal{D}_{JS}(p\|q) = -\frac{1}{2}(S[p] + S[q]) + S\left[\frac{p+q}{2}\right]. \quad (9)$$

Suppose that P is the distribution of the system to be analyzed and P_e is the equilibrium probability distribution for the number of possible states N, then the complexity using the Jensen-Shannon distance is known as the Martin-Plastino-Rosso (MPR) complexity [58,59],

$$C_{\mathrm{MPR}}[P] = Q_0 \cdot D_{JS}(P\|P_e) \cdot S[P], \quad (10)$$

where Q_0 is a normalization constant equal to the reciprocal of the maximum possible $\mathcal{D}_{JS}(P\|P_e)$ value, obtained when one of the components of P, e.g., p_j, is equal to one and the remaining components are zero:

$$Q_0 = -2\left(\frac{N+1}{(N+1) - \log(2N) + \log(N)}\right)^{-1}. \quad (11)$$

Note that the MPR complexity is also a normalized quantifier, $0 \leqslant C_{\mathrm{MPR}}[P] \leqslant 1$.

When plotting the behavior of statistical complexity, as seen in Fig. 9, three different behaviors can be observed for both ISR and NIAA for the three variations of the parameter c: A decrease in complexity for the intensity values ($D < 10^{-1}$), followed by a slight increase coinciding with the range of noise intensities, for which the particles are in the steady state and do not come out, and, once the noise intensity manages to bring them out of this state ($D > 10^{-1}$), a rapid decrease.

III. RESULTS

A. Inverse stochastic resonance

In order to study the behavior of the ISR in more detail and to gain a deeper understanding of the dynamics underlying the proposed model, we examine an asymmetric bistable potential. On the one hand, we have seen that the system is constrained to an asymmetric bistable potential, where the smallest activated potential is the least stable one, without any constraint on the width of the basin of attraction, as we can see in the main graph of Fig. 3. On the other hand, to obtain the probability function, we use the WEBDS method, which allows us not only to obtain the steady-state function ($D > 10^{-1}$), but also to show very well how it behaves in the regime with a low-noise-intensity regime ($D < 10^{-1}$). Figure 6(a) shows how the model correctly represents both behavioral regimes. In particular, in the low-intensity regime,
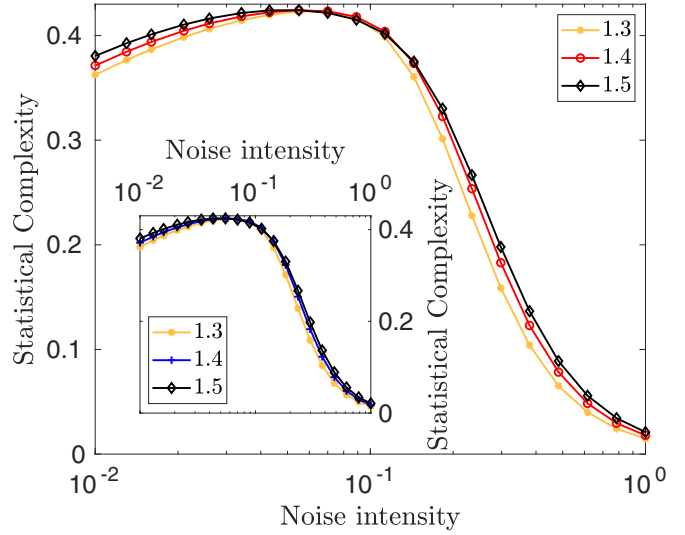
FIG. 9. Statistical complexity vs noise intensity for the ISR and NIAA regimes, respectively. There is a decrease in complexity up to values of noise intensity at which the barrier of the metastable state is completely overcome, and an increase in complexity while the intensity is insufficient to remove particles from the stable state.

it not only shows that the states become more similar when D is lower, but it also manages to better express the values of the local maximum.

B. Noise-induced activity amplification

Although the NIAA behavior is not well studied, we set out to investigate the properties of the system that generates this behavior in order to understand it and gain a deeper understanding of the underlying dynamics of the proposed model. We have shown that it is restricted only to an asymmetric bistable potential, where the stable state is the one with the highest activation, without any restriction on the width of the basin of attraction, as we can see in the inset of Fig. 3. We have also studied the probability function using the WEBDS method, which not only allows us to obtain this function in the stationary regime ($D > 10^{-1}$), but also shows very well how the probability behaves in the low-noise-intensity regime ($D < 10^{-1}$). Figure 6(b) shows how the model correctly represents both behavioral regimes. In particular, in the low-intensity regime, it not only shows that the states become more similar when D is lower, but it also succeeds in better expressing the values of the local maximum.

C. An information theoretic characterization of the fundamental neurocomputational features of ISR and NIAA

Some important aspects of brain activity, such as the ISR and NIAA, have specific functional characteristics for understanding information processing in the mammalian brain. To infer the relevance of information processing of both phenomena, we explore the activity patterns taking into account subtle measures of information: Shannon entropy, Fisher information, and MPR statistical complexity [43,44]. Determine the probability distribution function both for the limits of low

and high values of noise intensity and for their transition, and use this to estimate the emergent properties of these different neural structures quantifying the dynamic properties of the ISR-NIAA phenomenon. Figure 7 shows the information of Shannon entropy vs noise intensity, observing that for noise intensities higher than $D > 10^{-1}$, an increase to the chaotic state is typical, while for low intensity, the increase is interrupted by an abrupt decrease in noise-intensity values corresponding to the transition of the basin particles from the metastable state to the stable state. In contrast, in Fig. 8, where Fisher information is plotted against the intensity of the noise, the decay to the possible minimum is observed with a slight increase in the interval of the transition of the particles to the stable state. However, this change in behavior in this intensity interval is not seen in the behavior of the statistical complexity (Fig. 9) since it increases smoothly up to values close to $D \sim 10^{-1}$, where it remains stable until it drops abruptly at values $D > 10^{-1}$. The behavior of these magnitudes is maintained for both ISR and NIAA and for the different relations of the basin of attraction.

On the other hand, Fig. 10(a) shows the statistical complexity versus Shannon entropy for different values of the parameter c. Here the differences are between the behavior at low-noise intensity; the complexity remains around the value of 0.4 for the narrow entropy range [0.65, 0.75] (depending on the parameter c), while for higher-noise intensities, a direct decay to the state of maximum entropy and lower complexity is observed. Figure 10(b) shows Fisher information versus Shannon entropy, where the behavior of the entropy is more pronounced at low-noise intensity, i.e., the Fisher information remains practically constant, while the entropy increases due to the transition of the particles from the metastable minimum to the stable minimum. It also shows us that the smaller the area of attraction, the larger the value of the Fisher information. Finally, in Fig. 10(c), the Fisher information is plotted versus the statistical complexity, where a strong change in the Fisher information is observed once the maximum complexity is reached, with the particularity that less strong decreases are observed as the width of the basin of the metastable state decreases.

D. Different bistabilities

Next, we study how the shape of the potential $\varphi(x)$ affects the ISR and NIAA phenomena. Indeed, it has been reported that Purkinje cells can exhibit different amounts of bistability [35], which could represent diversity both within and between different zones of the cerebellum. Other authors suggest that the properties of Purkinje cells could be different in various cerebellar zones [60,61]. In addition, there is evidence that different biophysical mechanisms could regulate Purkinje cell bistability: For example, Bergmann glia (a neuron responsible for integrating the different signals of the cerebellar cortex and emitting the sole response of this system) could change the extracellular K^+ modulating Purkinje cell excitability [1].

Since there is different bistability in Purkinje cells, we analyze the existence of both phenomena and the properties of their behavior with the quantifiers of information theory for different bistable combinations resulting from different values
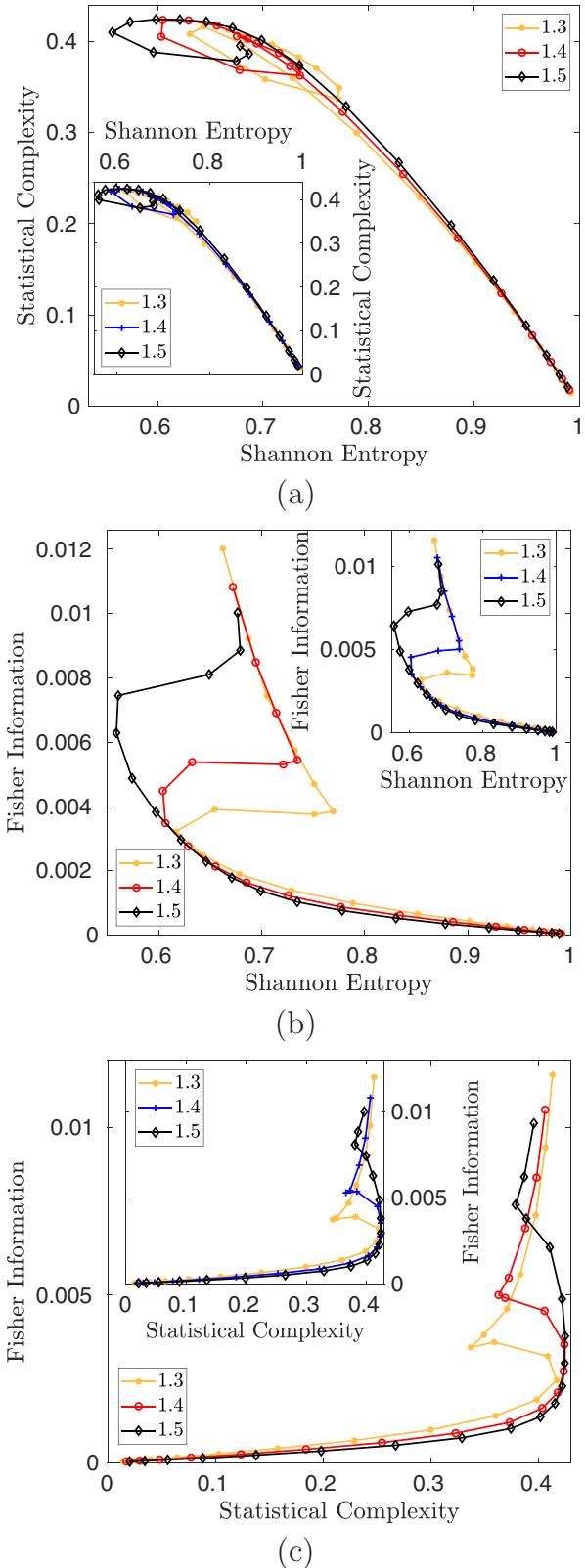
FIG. 10. Comparison between quantifiers: (a) statistical complexity vs Shannon entropy, (b) Fisher information vs Shannon entropy, and (c) Fisher information vs statistical complexity for the ISR and NIAA regimes, respectively.
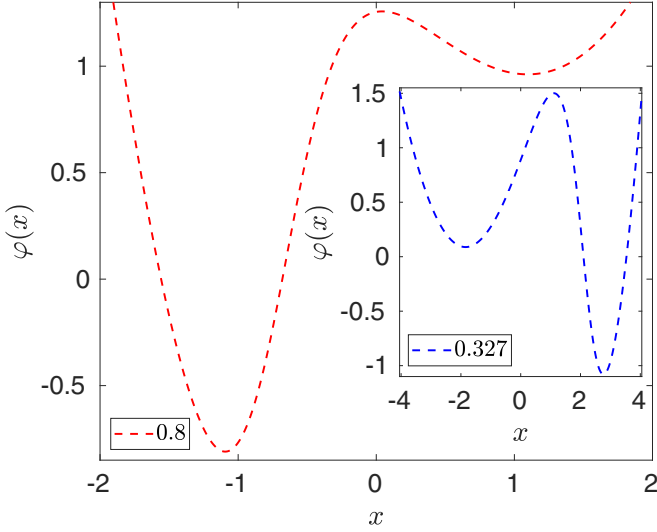
FIG. 11. Different potentials: ISR (dashed red line) for the parameters $a = 3.367$, $b = 2$, $c = 0.8$, $d = -3.337$, and $x_0 = 0.68$, and NIAA (dashed line blue) for $a = 4.367$, $b = -1.28$, $c = 0.327$, $d = 2.79$, and $x_0 = -2.1$.

of the parameters of $\varphi(x)$. In Fig. 11, we see two different combinations of potentials, one for ISR (red dashed line) and one for NIAA (blue dashed line). In both cases, compared to the potentials of Fig. 1, larger differences are observed both in the depths of the wells, $\Delta\varphi_{\text{down}}$ and $\Delta\varphi_{up}$, and in the widths of the basins of attraction, Δx_{down} and Δx_{up}.

If we start from the probability density function with WEBDS and compute the information theory quantifiers for these potentials, we observe the following: On the one hand, as can be seen in Fig. 12(a), with a linear increase of entropy up to the point where the noise intensity allows the particles to overcome the barrier of the metastable state, causing a decay up to the point where the noise intensity is sufficient for all particles to reach the stable state, for higher-noise intensities, the entropy increases its growth rate. Since the barriers of the metastable states are larger (dashed lines), there is a decrease in entropy at higher-noise intensities and a smaller decrease as the difference between the depth of the minima is smaller.

On the other hand, you can see in Fig. 12(b) the behavior of the Fisher information, where a short change in the behavior of the intensity values can be observed, where the metastable state is overcome, leading to changes in the growth tendency.

Finally, Fig. 12(c) shows the behavior of the statistical complexity, which reaches its maximum value at noise intensities that lie in the interval in which all particles are in the stable state, and up to the intensity at which the particles succeed in overcoming this state.

IV. CONCLUSIONS

Let us notice that most of the work presented here about ISR focused on a particular type of bistability, in which an oscillatory state coexists (limit cycle), alternating its occurrence in time, with a quiescent state in the presence of noise. Recently, an explanatory model for ISR was established [26],
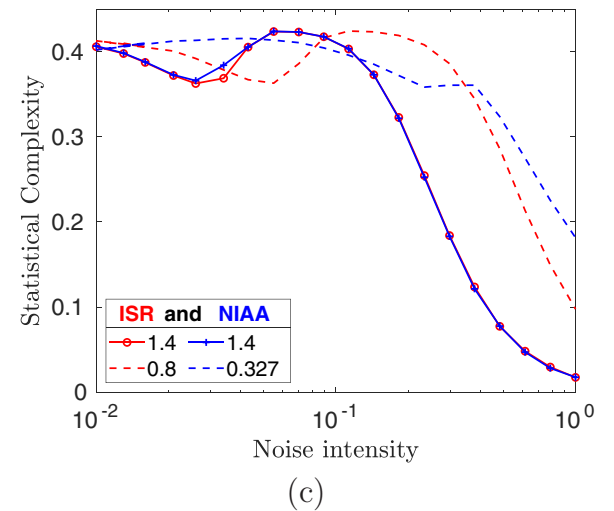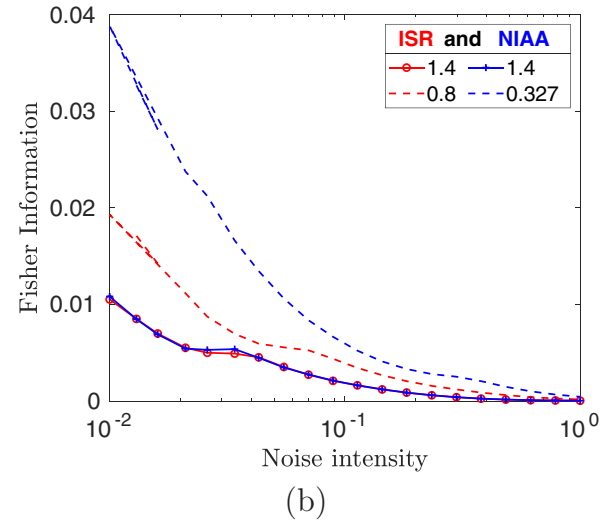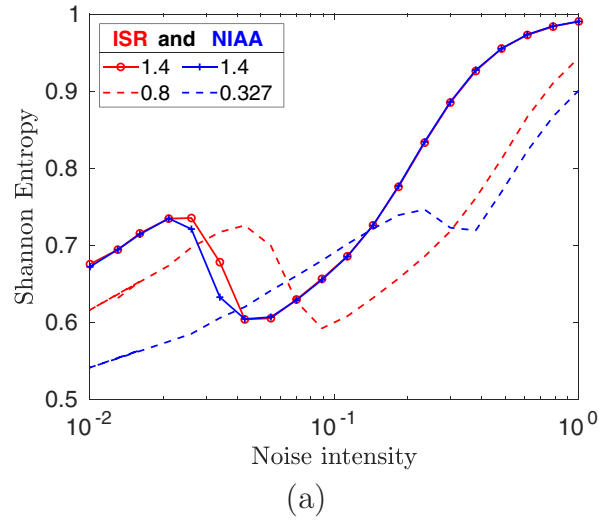
FIG. 12. Comparison of information theory quantifiers as a function of noise intensity: (a) Shannon entropy, (b) Fisher information, and (c) statistical complexity, for the potentials in Table I (solid lines) and Fig. 11 (dashed lines) potentials for ISR (red) and NIAA (blue).

which incorporates some key factors for the occurrence of interesting noise-induced effects. Among them is the coexistence of a stable rest equilibrium and a peak limit cycle that for the dynamics of neurons is indispensable since it is a suitable initial condition distribution [7,11]. This highlights the different nature of ISR with respect to SR, where initial conditions play no role, but also the procedures used to reveal the phenomenon are of relevance. Most of the relevant papers visualize the ISR phenomenon by calculating the average firing rate, which is an appropriate measure for the average activity of the system. In fact, the behavior of such an oscillatory system can, under appropriate assumptions, be reduced to that of the firing rate equations [31], whose dynamics is driven by the nonequilibrium potential, as can be found in Refs. [32,34]. That is, the bistability between a limit cycle and a rest state is reduced to a bistability between two single points in such rate models, one corresponding to a high firing rate and the other to a very small or null firing rate.

In this article, we deepen the theoretical basis explaining the occurrence of inverse stochastic resonance effects and noise-induced activity amplification in neural systems. To this end, we use the weighted-ensemble Brownian dynamics simulation model to determine the probability distribution function both for the limits of low and high values of noise intensity and for intermediate-noise intensities, to show that ISR occurs in any system whose dynamics can be interpreted as a potential function with two minima, one of which is metastable with the highest activity and the other with the global minimum. On the other hand, the metastable state must be less active than the global minimum for the NIAA effect to occur, in both cases, without the peculiarities between the sizes of the basins of attraction. The application of this method also allows us to obtain the probability function to analyze these phenomena using the quantifiers provided by information theory.

In summary, the analysis of Shannon entropy as a function of noise intensity allows us to identify the ISR and NIAA behavior when the noise intensity decreases and the particles

manage to jump from the metastable state to the stable state, showing that the system is provisionally ordered but continues to be disordered when the noise intensity further increases. On the other hand, both Fisher information and statistical complexity show different behavior in the same intensity interval, as Fisher information decreases slightly and the complexity increases uniformly. For values of the noise intensity at which it is possible to overcome the barrier of the stable state, the particles can be in any part of the system, reflecting the tendency toward the maximum values of the Shannon entropy and the minimum values of the Fisher information and statistical complexity.

Surprisingly, our results show that Fisher information increases as the system reaches ISR and NIAA states, while Shannon entropy decreases in a more ordered state and statistical complexity increases. In particular, we can see that for certain values of the potential [e.g., Fig. 12(b), 0.8], the Fisher information is larger in the case of ISR than in the case of 1.4 with NIAA, showing that the intrinsic behavior of bistability can lead us to more efficient information transmission in certain cases. Although these results are not universal, since in some cases the opposite case is observed, where NIAA shows more efficient information transmission than ISR, we believe that it is very important to take into account the bistable nature of Purkinje cells since they could control information transmission using ISR or NIAA, depending on the biological process that may be associated with the emergent properties of the system.

[1] F. Wang, Q. Xu, W. Wang, T. Takano, and M. Nedergaard, Proc. Natl. Acad. Sci. USA **109**, 7911 (2012).

[2] C. Oldfield, A. Marty, and B. Stell, Proc. Natl. Acad. Sci. USA **107**, 13153 (2010).

[3] A. Buchin, S. Rieubland, M. Häusser, B. S. Gutkin, and A. Roth, PLoS Comput. Biol. **12**, e1005000 (2016).

[4] S. R. Schultz, Scholarpedia **2**, 2046 (2007).

[5] B. S. Gutkin, J. Jost, and H. C. Tuckwell, Theory Biosci. **127**, 135 (2008).

[6] H. C. Tuckwell, J. Jost, and B. S. Gutkin, Phys. Rev. E **80**, 031907 (2009).

[7] B. S. Gutkin, J. Jost, and H. C. Tuckwell, Naturwissenschaften **96**, 1091 (2009).

[8] D. Guo, Cognit. Neurodyn. **5**, 293 (2011).

[9] H. C. Tuckwell and J. Jost, J. Comput. Neurosci. **30**, 361 (2011).

[10] M. Uzuntarla, Phys. Lett. A **377**, 2585 (2013).

[11] M. Uzuntarla, J. R. Cressman, M. Ozer, and E. Barreto, Phys. Rev. E **88**, 042712 (2013).

[12] W. Braun, P. C. Matthews, and R. Thul, Phys. Rev. E **91**, 052701 (2015).

[13] M. E. Yamakou and J. Jost, Europhys. Lett. **120**, 18002 (2017).

[14] B. A. Schmerl and M. D. McDonnell, Phys. Rev. E **88**, 052722 (2013).

[15] D. Guo, M. Perc, T. Liu, and D. Yao, Europhys. Lett. **124**, 50001 (2018).

[16] M. Uzuntarla, E. Barreto, and J. J. Torres, PLoS Comput. Biol. **13**, e1005646 (2017).

[17] A. S. Pikovsky and J. Kurths, Phys. Rev. Lett. **78**, 775 (1997).

[18] A. A. Faisal, L. P. Selen, and D. M. Wolpert, Nat. Rev. Neurosci. **9**, 292 (2008).

[19] B. Lindner, J. García-Ojalvo, A. Neiman, and L. Schimansky-Geier, Phys. Rep. **392**, 321 (2004).

[20] M. Perc, Phys. Rev. E **76**, 066203 (2007).

[21] M. Ozer, M. Perc, and M. Uzuntarla, Phys. Lett. A **373**, 964 (2009).

[22] L. Gammaitoni, P. Hänggi, P. Jung, and F. Marchesoni, Eur. Phys. J. B **69**, 1 (2009).

[23] M. D. McDonnell and D. Abbott, PLoS Comput. Biol. **5**, e1000348 (2009).

[24] M. c. v. Perc and M. Marhl, Phys. Rev. E **71**, 026229 (2005).

[25] L. Gammaitoni, P. Hänggi, P. Jung, and F. Marchesoni, Rev. Mod. Phys. **70**, 223 (1998).

[26] J. J. Torres, M. Uzuntarla, and J. Marro, Commun. Nonlinear Sci. Numer. Simulat. **80**, 104975 (2020).

[27] I. Bačić, V. Klinshov, V. Nekorkin, M. Perc, and I. Franović, Europhys. Lett. **124**, 40004 (2018).

[28] I. Bačić and I. Franović, Chaos **30**, 033123 (2020).

[29] A. Zamani, N. Novikov, and B. Gutkin, Commun. Nonlinear Sci. Numer. Simulat. **82**, 105024 (2020).

[30] R. Barrio, S. Coombes, M. Desroches, F. Fenton, S. Luther, and E. Pueyo, Commun. Nonlinear Sci. Numer. Simulat. **86**, 105275 (2020).

[31] N. Brunel, J. Comput. Neurosci. **8**, 183 (2000).

[32] G. G. Izús, R. R. Deza, and H. S. Wio, Phys. Rev. E **58**, 93 (1998).

[33] H. S. Wio, R. R. Deza, and J. M. López, *An Introduction to Stochastic Processes and Nonequilibrium Statistical Physics, revised ed.* (World Scientific, Singapore, 2012).

[34] R. R. Deza, J. I. Deza, N. Martínez, J. F. Mejías, and H. S. Wio, Front. Phys. **6**, 154 (2019).

[35] B. Alberts, A. Johnson, J. Lewis, M. Raff, K. Roberts, and P. Walter, *Molecular Biology of the Cell* (Garland Science, New York, 2002).

[36] A. Becskei, B. Seraphin, and L. Serrano, EMBO J. **20**, 2528 (2001).

[37] J. J. Tyson, K. C. Chen, and B. Novak, Curr. Opin. Cell Biol. **15**, 221 (2003).

[38] D. Frigola, L. Casanellas, J. M. Sancho, and M. Ibañes, PLoS ONE **7**, e31407 (2012).

[39] N. G. Van Kampen, *Stochastic Processes in Physics and Chemistry* (Elsevier, New York, 2007), 3rd ed., Vol. 1.

[40] K. Voigtlaender and H. Risken, J. Stat. Phys. **40**, 397 (1985).

[41] J. A. Kromer, L. Schimansky-Geier, and R. Toral, Phys. Rev. E **87**, 063311 (2013).

[42] C. Shannon and W. Weaver, *The Mathematical Theory of Communication* (University of Illinois Press, Champaign, IL, 1949).

[43] O. A. Rosso and C. Masoller, Phys. Rev. E **79**, 040106(R) (2009).

[44] O. A. Rosso and C. Masoller, Europhys. J. B **69**, 37 (2009).

[45] N. Lotfi, T. Feliciano, L. A. A. Aguiar, Thais Priscila Lima Silva, T. T. A. Carvalho, O. A. Rosso, M. Copelli, F. S. Matias, and P. V. Carelli, Phys. Rev. E **103**, 012415 (2021).

[46] M. Granado, S. Collavini, R. Baravalle, N. Martinez, M. A. Montemurro, O. A. Rosso, and F. Montani, Chaos: Interdiscip. J. Nonlin. Sci. **32**, 093151 (2022).

[47] B. Frieden, *Science from Fisher Information: A Unification* (Cambridge University Press, Cambridge, UK, 2004).

[48] P. Sánchez-Moreno, R. Yánez, and J. Dehesa, in *Proceedings of the 14th International Conference on Difference Equations and Applications*, edited by M. Bohner, Z. Dosla, G. Ladas, M. Unal, and A. Zafer (Bahçeşehir University Press, Istanbul, 2009), pp. 291–298.

[49] F. Montani and O. A. Rosso, Entropy **16**, 4677 (2014).

[50] R. Lopez-Ruiz, H. L. Mancini, and X. Calbet, Phys. Lett. A **209**, 321 (1995).

[51] D. Bhatt and I. BaharIzhikevich, J. Chem. Phys. **137**, 104101 (2012).

[52] S. Kullback and R. A. Leibler, Ann. Math. Statist. **22**, 79 (1951).

[53] C. Tsallis, *Introduction to Nonextensive Statistical Mechanics* (Springer, New York, 2009).

[54] A. Rényi, in *Proceedings of the Fourth Berkeley Symposium on Mathematical Statistics and Probability, Volume 1 Contributions to the Theory of Statistics* (University of California Press, 1961), Vol. 4, pp. 547–562.

[55] W. K. Wootters, Phys. Rev. D **23**, 357 (1981).

[56] I. Grosse, P. Bernaola-Galván, P. Carpena, R. Román-Roldán, J. Oliver, and H. E. Stanley, Phys. Rev. E Stat. Nonlin. Soft Matter Phys. **65**, 041905 (2002).

[57] F. Montani, O. A. Rosso, and S. R. Schultz, AIP Conf Proc. **913**, 184 (2007).

[58] M. T. Martin, A. Plastino, and O. A. Rosso, Physica A **369**, 439 (2006).

[59] O. A. Rosso, H. A. Larrondo, M. T. Martín, A. Plastino, and M. A. Fuentes, Phys. Rev. Lett. **99**, 154102 (2007).

[60] L. Witter and C. I. De Zeeuw, Curr. Opinion Neurobiol. **33**, 150 (2015).

[61] H. Zhou, K. Voges, Z. Lin, C. Ju, and M. Schonewille, J. Neurophysiol. **113**, 2524 (2015).